Hindawi Publishing Corporation
Mathematical Problems in Engineering
Volume 2015, Article ID 324961, 15 pages
http://dx.doi.org/10.1155/2015/324961

Research Article

Numerical Assessment of Similitude Parameters and Dimensional Analysis for Water Entry Problems

Andrea L. Facci and Stefano Ubertini

School of Engineering, University of "Tuscia", 01100 Viterbo, Italy

Correspondence should be addressed to Andrea L. Facci; andrea.facci@unitus.it

Received 5 April 2015; Accepted 19 May 2015

Academic Editor: Anna M. Gil-Lafuente

The prediction of impulsive loads deriving from the sudden impact of a solid body on the water surface is of fundamental importance for a wide range of engineering applications. The study of hull-slamming phenomena largely relies on laboratory scale experimental investigations and on simplified analytical models. The aim of this paper is to quantitatively assess the interplay between the relevant nondimensional parameters for the water entry of a two-dimensional body, evidencing the similitude conditions that allow the transition from scaled experiments to real size applications. This assessment is performed through the numerical study of the hydrodynamics induced by the water impact of a two-dimensional wedge. The fluid flow is considered incompressible. First of all numerical simulations are validated by comparison with experimental data from the literature and with the Wagner seminal theory. Afterwards, a thorough computational study is performed by systematically varying all the relevant parameters, such as the nondimensional entry velocity and acceleration. We conclude by evidencing some design prescriptions that should be adopted in order to facilitate the transition of laboratory scale experiments to real scale applications.

1. Introduction

The prediction of the impulsive loading originating from the impact between a body and the water surface, often referred to as hull slamming, is considered one of the most challenging aspects for the design of vessel shells and off-shore structures [1]. In fact, water impact can easily generate large stresses that, in turn, may cause severe structural damages [2–4]. Thereof, the probability and the intensity of the slamming events are among the most relevant issues for the determination of the operational limit for ships (i.e., the navigation velocity) [1].

Water entry problems have been the object of significant research efforts starting from the seminal analytical works of Von Karman [5] and Wagner [6]. Analytical approaches are effective in capturing the forces and the pressure distribution under geometrical (i.e., two-dimensionality, symmetry, or low deadrise angle) and flow (i.e., inviscid) constraints [1, 7–13]. On the other hand, numerical [14–19] and experimental [3, 4, 20–24] studies have been performed to understand the flow physics underlying hull slamming under more general shapes as well as flow conditions [18, 25]. In particular, in [4, 26] a nonintrusive procedure for the evaluation of the hydrodynamic pressure is developed and validated. The impulsive nature of the phenomenon, together with the necessity to capture the correct evolution of the water-air interface, probably represent the most demanding issues for both numerical and experimental procedures.

Numerical as well as physical experiments are usually performed on laboratory scale models (see, e.g., [4, 17, 22]) in order to reduce the experimental facility costs or calculation time. Thereafter, the assessment of a proper methodology to reproduce real world problems at a laboratory scale, could boost the utilization of existing as well as new experimental results for the design of structures subject to significant slamming events. This methodology relies on the identification of relevant nondimensional parameters that define the physical similarity conditions through the Buckingham theorem [27]. Moreover, the utilization of nondimensional parameters allows reducing the number of trials necessary for each experimental campaign [27]. However, in most cases,

it is not possible to guarantee a strict similitude with all the nondimensional parameters held to be the same for both the scale model and the real application. In these cases the validity of the scale tests is still ensured, if some aspects of the similitude can be neglected or a departure from the real-world operating conditions is acceptable within certain limits. Such an investigation for water entry problems is still missing in the literature.

In this paper, we investigate the influence of the relevant nondimensional parameters on hull slamming events, with particular attention to the hydrodynamic loading exerted by the water during the impact. The analysis is focused on the different flow regimes produced by the variation of inertia and acceleration and is carried out by studying the water entry of a two-dimensional (2D) wedge through computational fluid dynamics (CFD). The aim of this study is to quantitatively assess the similitude conditions that allow the transition from laboratory to real scale applications.

The paper is organized as follows. The physical problem is described in Section 2. Therein nondimensional parameters are identified and explained in detail. The numerical method is described and validated in Section 3, and results are presented and analyzed in Section 4. Conclusions are highlighted in Section 5.

2. Problem Statement

We numerically study the water entry problem of a two-dimensional rigid wedge schematically depicted in Figure 1. Therein, the following geometrical parameters are reported: (i) the wedge width L; (ii) the deadrise angle β; (iii) the keel penetration with respect to the undisturbed water level ξ; (iv) the reference wet length $\tilde{r}$, that is, the abscissa identified by the intersection of the undisturbed water level with the wedge surface; and (v) the reference wet surface $A = \xi/\sin(\beta)$. A Cartesian reference frame is placed with the y-axis oriented downward along the vertical direction and with the origin corresponding to the undisturbed water level at time $t = 0$. The main features of the impact hydrodynamics, such as the effective wet length r, the jet spray, and the jet root regions, are also illustrated.

At $t = 0$ the keel of the rigid wedge is placed at $y = 0$ (i.e., at the undisturbed water level) and the body is allowed to fall with an initial vertical velocity v_0. Afterwards, a predetermined vertical motion, characterized by a constant deceleration a, is imposed to the wedge to highlight the effects of v_0 and a on the impact induced hydrodynamics. Since v_0 is much lower compared to the speed of sound in the water (c_s), in particular the maximum ratio v_0/c_s is about 10^{-3}, the flow is assumed to be incompressible. The incompressible flow generated by the impact of the wedge on the water is described by the mass conservation and the Navier Stokes equations reported in

$$\nabla \cdot \mathbf{u} = 0, \tag{1a}$$

$$\frac{\mathrm{D}\rho\mathbf{u}}{\mathrm{D}t} = -\nabla p + \nabla \cdot (\mu \nabla \mathbf{u}) + \rho \mathbf{g}, \tag{1b}$$

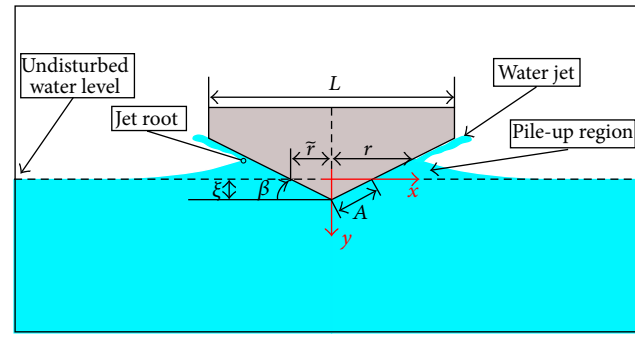

Figure 1: Schematic of the water entry problem and of the relevant geometrical parameters.

where $\mathbf{u}$ is the fluid velocity, p is the pressure, ρ and μ are the water density and viscosity, and $\mathrm{D}/\mathrm{D}t$ represents the material derivative. Thereafter, the physical parameters that characterize the slamming event are the vertical force F, the pressure field p acting on the wedge surface, and the wet length r. In turn, those parameters vary with the time t as functions of v_0, L, β, ρ, μ, and of the abscissa x. Thereof, it is possible to resort to the nondimensional numbers reported in Table 1 to gain a complete description of the water entry problem. In this framework, we consider the nondimensional force c_F, the pressure coefficient c_p, and the pile-up coefficient ϕ as dependent parameters. The deadrise angle β, the nondimensional time τ, the nondimensional abscissa χ, and the two dimensionless groups, Re and Fr, are independent variables. Specifically, we will focus on the competition between the inertia of the wedge at the impact and the viscous forces through the Reynolds number, defined as

$$\mathrm{Re} = \frac{\rho v_0 L}{\mu}, \tag{2}$$

and on the relative importance of the inertia force with respect to external forces through a dimensionless acceleration, which can be referred to as a generalized Froude number:

$$\mathrm{Fr} = \frac{v_0}{\sqrt{aL}}. \tag{3}$$

3. Numerical Method

3.1. Free Surface Flow Modeling. The numerical simulations are performed using the interDyMFoam solver from the OpenFOAM-2.2 software package [28] which uses the Volume of Fluid (VOF) method [29–32] to numerically describe the incompressible flow of two immiscible fluids. According to this methodology, a single set of the Navier-Stokes and continuity equations (see (1a) and (1b)) is solved for both phases (i.e., air and water). The evolution of the interface between the two phases is reconstructed by solving the

Table 1: Relevant nondimensional parameters for the incompressible two-dimensional water entry problem.

Force coefficient	Pressure coefficient	Pileup coefficient	Deadrise angle
$c_F = \frac{-F}{1/2\rho A v_0^2}$	$c_p = \frac{p}{1/2\rho v_0^2}$	$\phi = \frac{r}{\tilde{r}}$	β
Time coefficient	Reynolds number	Froude number	Nondimensional abscissa
$\tau = \frac{v_0 t}{L\tan(\beta)}$	$\mathrm{Re} = \frac{\rho v_0 L}{\mu}$	$\mathrm{Fr} = \frac{v_0}{\sqrt{aL}}$	$\chi = \frac{x}{r}$

following equation for the liquid phase volume fraction [32, 33]:

$$\frac{\mathrm{D}\alpha}{\mathrm{D}t} = 0. \tag{4}$$

The resulting system of partial differential equations is discretized using the finite volume technique [34]. The pressure velocity coupling is performed through the noniterative Pressure Implicit with Split Operators (PISO) algorithm [35], while the discretized version equation (4) is solved using the Multidimensional Universal Limiter with Explicit Solution (MULES) procedure [36]. Temporal discretization is performed through the second-order accurate implicit backward scheme [36], and the Gauss linear procedure is adopted for all the spatial interpolations, other than the convective terms, where the Gauss gamma scheme [37] is adopted balance numerical stability and accuracy. All the resulting linear systems are solved using the geometric agglomerated algebraic multigrid iterative algorithm [36].

Special turbulence modeling is not required for the numerical solution of the hull-slamming problem. In fact, the impulsive nature of the water entry related phenomena does not allow the development of a proper energy cascade as demonstrated in [16]. The same consideration applies also for three-dimensional effects [16] that may only derive from edge effects that can be safely discarded when the transversal dimension of the falling body is much larger than the other ones, as we assume, without losing generality, in the present study.

The computational domain is discretized using the structured multiblock mesh represented in Figure 2. Specifically, 125 grid cells are placed on the wet side of the wedge, and the mesh is made of about 4×10^4 cells. Moreover, we exploited the problem symmetry to reduce the computational cost of the numerical experiments by simulating only half of the domain. As evidenced in Figure 2(c), besides the symmetry condition on the left side of the domain, no-slip boundary conditions are imposed to the wedge walls, $p = 0$ pressure inlet is imposed to the top boundary, and, finally, the free-slip condition is imposed to all the other boundaries. A thorough description of the boundary conditions implementation is given in [38].

The wedge motion inside the computational domain is allowed to reallocate the mesh nodes after each time step, without the necessity of topological changes. The grid deformation is performed using the Laplace smoothing methodology [39–41].

The vertical force acting on the wedge surface is calculated by numerically integrating the stress tensor $\mathbf{T} = -p\mathbf{I} + \mu[\nabla\mathbf{u} + (\nabla\mathbf{u})^T]$ and projecting the result along the y-axis. Numerical integration is performed through the following second-order accurate formulation:

$$F = \left(\sum_{i=1}^{N_w} \mathbf{T}_i \mathbf{n}_i \Sigma_i\right) \cos(\beta), \tag{5}$$

where N_w is the number of cells employed to discretize the wedge surface, Σ_i is the area of a generic surface element, and $\mathbf{n}_i$ is the unit vector normal to the surface element.

3.2. Validation. The validation of the numerical procedure adopted throughout the paper is provided comparing numerical results with experimental pressure profiles from [4]. Therein the hydrodynamic pressure acting on a free falling wedge is experimentally measured using a nonintrusive procedure based on particle image velocimetry (PIV). More in detail, in [4], a 200 mm large and 220 mm width specimen, characterized by a mass of 0.425 kg, was allowed to fall from 0.5 m above the water surface. The resulting impact velocity was about 3 m/s.

Since this paper concentrates on the prediction of the hydrodynamic loading deriving from well-defined solid body motion, the wedge free fall is numerically emulated by imposing the experimentally measured velocity time series to the wedge. The resulting pressure on the wedge is compared to its experimental counterpart in Figure 3, confirming the fidelity of the utilized methodology. In particular, a substantial agreement on the pressure values close to the wedge keel and on the c_p minimum position is evidenced. The differences between experimental and numerical c_p are localized within a relatively small region close to the jet root where the experimental results are less accurate due to the unavoidable reflection of the PIV laser sheet at the liquid-air interface [4].

4. Results and Discussion

4.1. Comparison with the Analytical Model. In this section, we compare numerical results to the Wagner analytical model [6], which is based on the potential flow theory, neglects gravity, and is nominally applicable to small deadrise angles. In particular, according to the Wagner solution, the pressure coefficient on the wet side of the wedge can be computed as

$$c_{p_w} = \frac{2}{v_0}\left[-a\sqrt{r_w^2 - x^2} + \frac{\pi}{2}\frac{\dot{\xi}^2 r}{\tan(\beta)\sqrt{r_w^2 - x^2}} - \frac{1}{2}\frac{\dot{\xi}^2 x^2}{r_w^2 - x^2}\right], \tag{6}$$

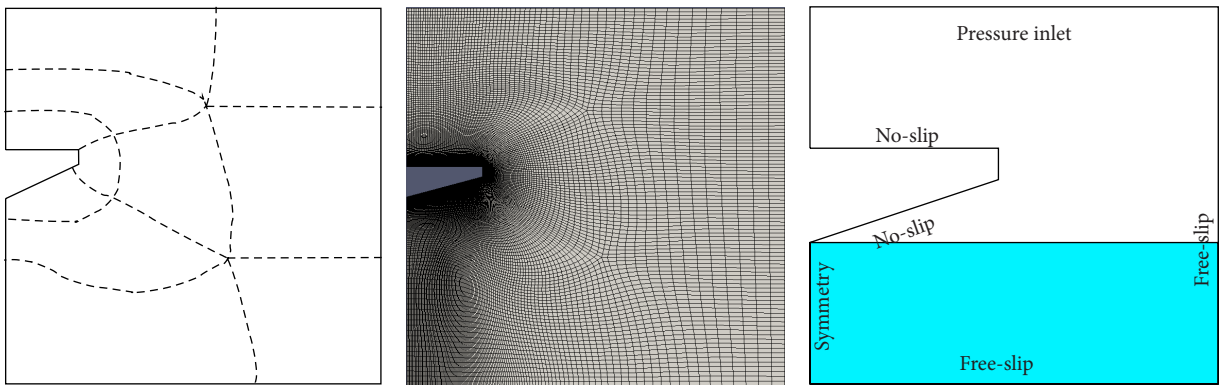

(a) Mesh topology (b) Mesh representation (c) Boundary conditions

Figure 2: Schematic of the computational domain with the indication of: (a) mesh topology; (b) mesh representation; and (c) boundary conditions.

where $r_w = \pi\xi/(2\tan(\beta))$ is the wet length and a superimposed dot denotes the time derivative.

Numerical and analytical pressure profiles are compared in Figures 4 and 5 for different deadrise angles within the range $[15^\circ, 35^\circ]$. Therein, $\mathrm{Re} = 10^6$ is considered to approximate the hypothesis of inviscid flow, underlying Wagner's solution, and the water impact is simulated considering both a constant penetration velocity (see Figure 4) and a uniformly decelerated motion (see Figure 5). It is observed that the computed c_p is well in line with the theoretically predicted profile for both $\beta = 15^\circ$ and $\beta = 25^\circ$, when $\mathrm{Fr} = \infty$. As expected, increasing β up to 35° (see Figure 4(c)), computed c_p significantly differs from the Wagner solution as the small deadrise angle hypothesis is not fully respected.

Notably, for $\beta = 35^\circ$, according to CFD, c_p minimum is found for $x > 0$, while (6) is minimized at $x = 0$. Moreover, in the latter case, the numerically computed c_p is considerably lower compared to the Wagner prediction. On the other hand, the wedge deceleration emphasizes the discrepancy between CFD and analytical pressure profile. In fact, for $\mathrm{Fr} = 0.5$, a remarkable difference between CFD and Wagner's results is already detected for $\beta = 25^\circ$, as shown in Figure 5. This difference is particularly evident at the keel, where the pressure coefficient predicted by the numerical model is significantly higher than the analytical one.

4.2. Influence of the Nondimensional Parameters. The penetration velocity and acceleration are systematically varied in the range $[5 \times 10^{-3}, 5]$ m/s and $[0, 100]$ g, respectively, to elucidate their effects on the impact related hydrodynamics. Specifically, Table 2 summarizes the set of the simulations that are performed, evidencing both their physical and nondimensional characteristic parameters. It is noted that $\mu = 10^{-6}$ kg/ms, $L = 0.2$ m, $\rho = 1000$ kg/m^3, and $\beta = 25^\circ$, for all the test cases. To garner insight into the effects of these parameters three groups of simulations are considered: (i) constant $\mathrm{Fr} = \infty$ and varying Re; (ii) constant $\mathrm{Fr} = 0.5$ and varying Re; and (iii) constant $\mathrm{Re} = 10^6$ and varying Fr.

Table 2: Summary of the numerical test cases.

		v_0 [m/s]			
		5×10^{-3}	5×10^{-2}	5×10^{-1}	5
a [m/s^2]	0.0	Re= 10^3 Fr = ∞	Re= 10^4 Fr = ∞	Re= 10^5 Fr = ∞	Re= 10^6 Fr = ∞
	1×10^{-4} g	Re = 10^3 Fr = 0.5			
	1×10^{-2} g		Re = 10^4 Fr = 0.5		
	0.5 g				Re = 10^6 Fr = 7.1
	g			Re = 10^5 Fr = 0.5	Re = 10^6 Fr = 5.0
	5 g				Re = 10^6 Fr = 2.3
	10 g				Re = 10^6 Fr = 1.6
	50 g				Re = 10^6 Fr = 0.7
	100 g				Re = 10^6 Fr = 0.5

4.2.1. Reynolds Number Influence. As evidenced in Table 2, the Reynolds number is varied within a wide range (i.e., $[10^3$–$10^6]$) that allows dissecting the interplay between different physical phenomena, such as viscous and inertia related forces. In fact, as Re is increased the influence of viscous forces is expected to vanish, as compared to inertial and pressure effects. This effect is clearly evidenced by the results reported in Figure 6(a) that depicts the c_F trend as a function of τ for different Reynolds numbers and with a constant penetration velocity.

It is noted that, for $\mathrm{Re} = 10^3$, c_F is influenced by τ, or equivalently by the effective wedge penetration, throughout the whole τ range. On the other hand, for $\mathrm{Re} \geq 10^4$, c_F is

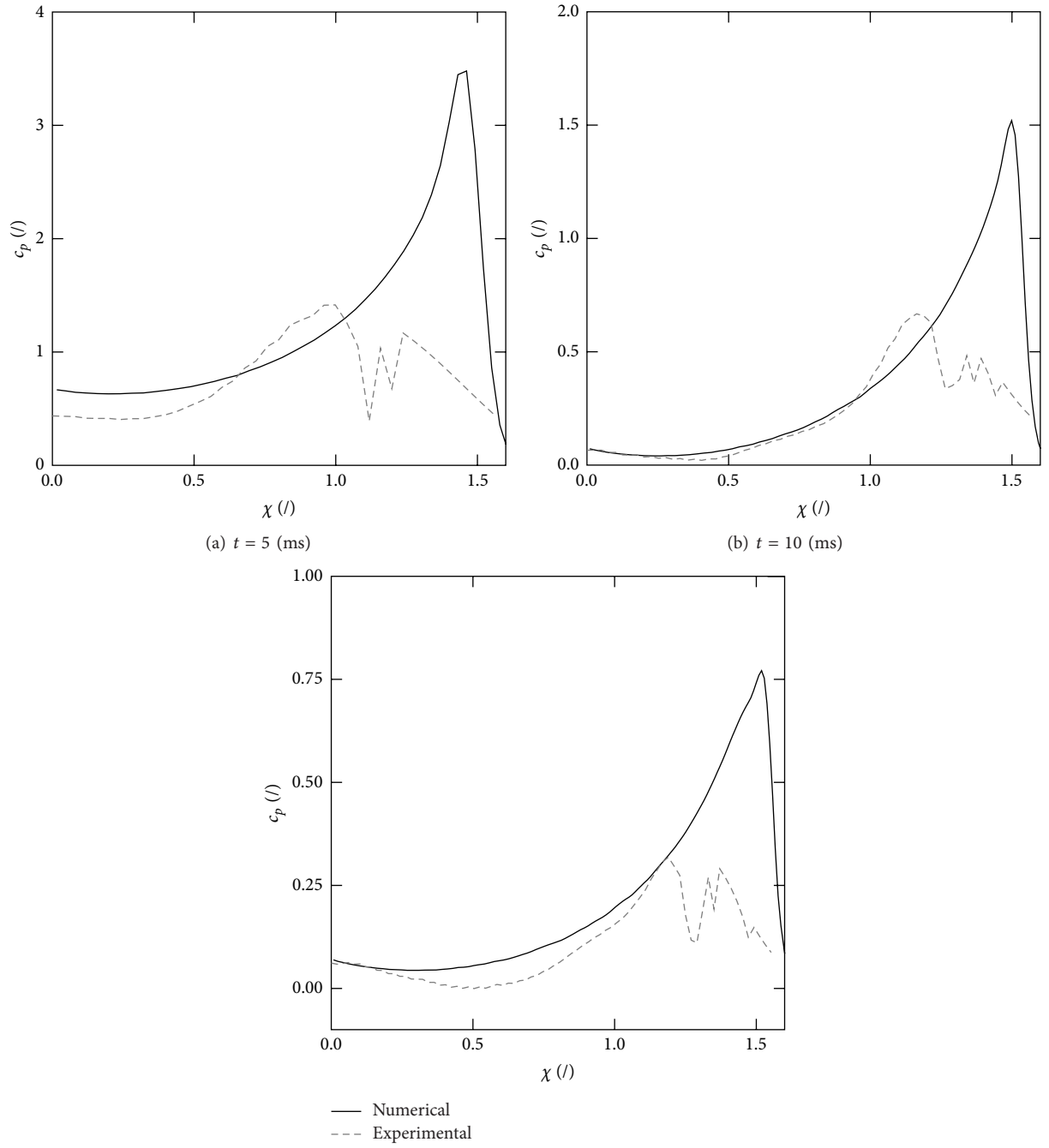

(a) $t = 5$ (ms)

(b) $t = 10$ (ms)

(c) $t = 15$ (ms)

Figure 3: Comparison of numerical and experimental pressure profiles [4] on the wet surface for different time-steps. (a) $t = 5$ (ms); (b) $t = 10$ (ms); and $t = 15$ (ms).

no more influenced by the wedge penetration for τ greater than approximately 1/3. Notably, in the latter flow regime, all the c_F curves collapse to roughly the same values. On the contrary, for lower values of τ, a nonnegligible effect of Re can be observed also for Re as high as 10^5-10^6. This behavior is related to the fact that at the onset of the impact, which is to say at low τ, the portion of the wedge length effectively in contact with the water is very limited. Therefore, the mass of water displaced by the wedge, and, consequently, the fluid inertia, is relatively low, thus making viscosity effects significant. We further comment that each simulation is performed until the wedge is completely submerged in water, and the maximum value for τ is lower than one as a consequence of the water pile-up.

Further insight on the interplay between viscous and inertial phenomena can be garnered by comparing the pressure

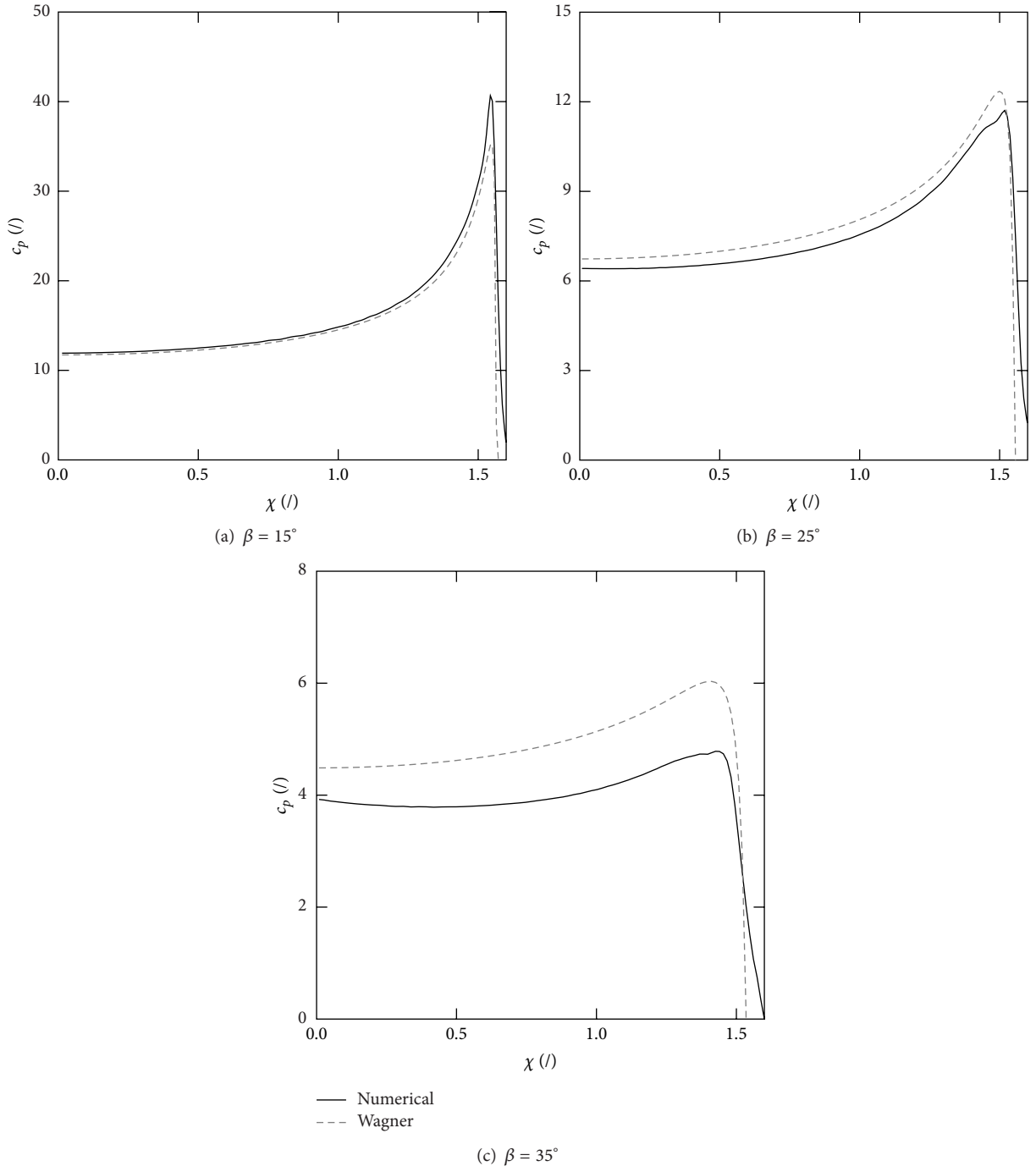

FIGURE 4: Comparison of analytical and numerical pressure profiles on the wet surface for Re = 10^6, Fr = ∞, and different deadrise angles, as a function of the dimensionless abscissa. (a) $\beta = 15^\circ$; (b) $\beta = 25^\circ$; and (c) $\beta = 35^\circ$.

profiles, along the wet side of the wedge, reported in Figure 6(b), where we clearly observe that the pressure coefficient is almost independent of the Reynolds number. Thereafter, the variation of the hydrodynamic forces with the Reynolds number is to be ascribed to viscous effects. It is also worth noting that, in Figure 6(b), c_p is represented for a single value of τ as the pressure distribution over the wedge is expected to be self-similar in time for a constant velocity penetration [4, 6]. The pressure acting on the wedge can also be argued from Figure 7 that represents the pressure contour plot in the vicinity of the wedge for Fr = ∞, as a function of τ and Re. It is therein evidenced that the pressure field does not vary significantly in the range Re = $[10^3, 10^6]$.

Figure 6(c) shows the variation of the pile-up coefficient ϕ as a function of τ and Re. The pile-up coefficient is estimated from the pressure profiles by hypothesizing that the jet root

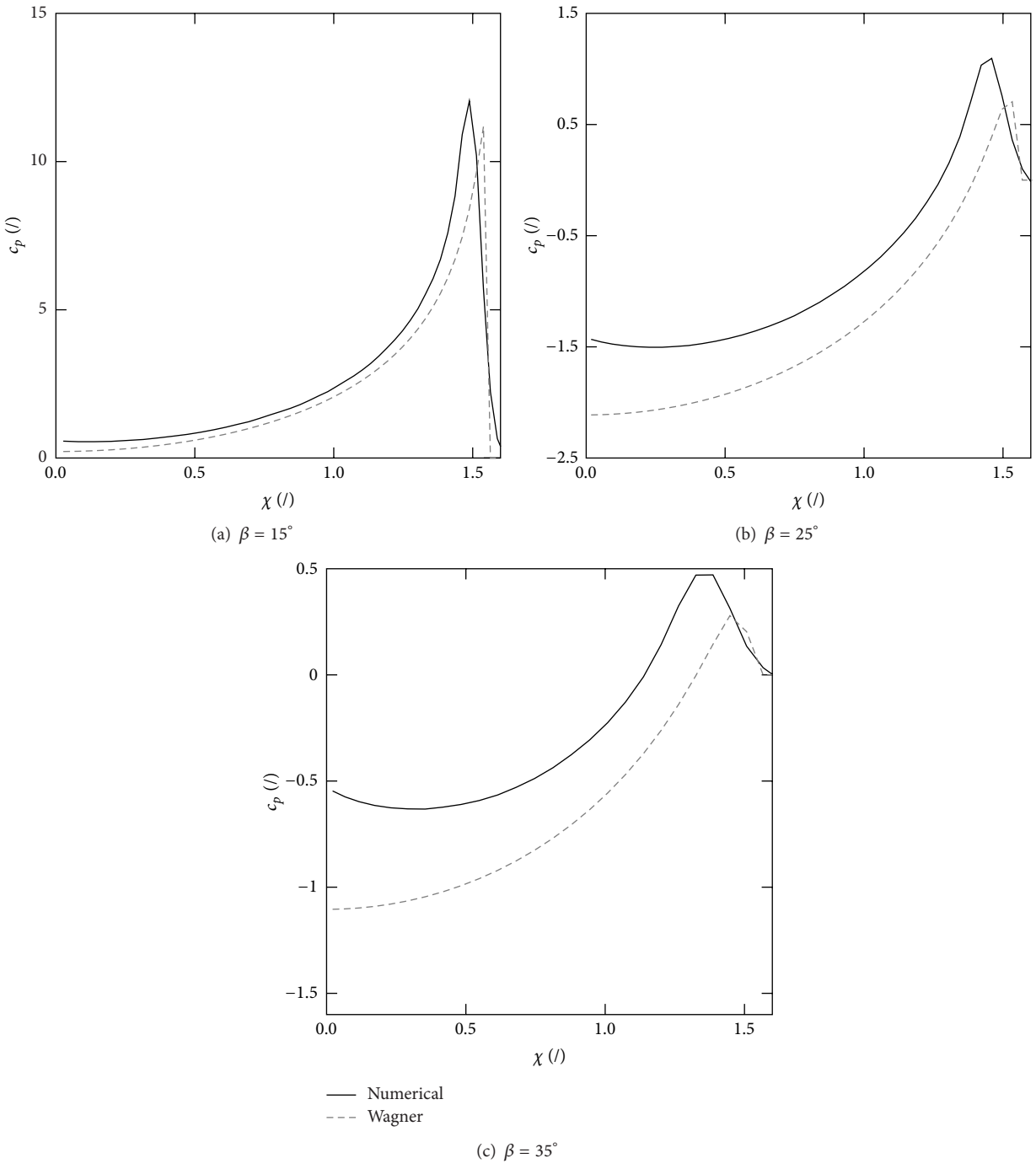

FIGURE 5: Comparison of analytical and numerical pressure profiles on the wet surface for Re = 10^6, Fr = 0.5, and different deadrise angles, as a function of the dimensionless abscissa. (a) $\beta = 15^\circ$; (b) $\beta = 25^\circ$; and (c) $\beta = 35^\circ$.

location corresponds to the pressure peak on the wedge. Thereafter, we evaluate r as the abscissa of the pressure peak along the wedge. The water jets can also be easily detected in Figure 8 that depicts the contour plot of the liquid volume fraction, α, as a function of τ and Re, and for Fr = ∞. It is noted that the air-water interface position corresponds to the relatively narrow transition from $\alpha = 1$ to $\alpha = 0$. This diffused interface that is spread across few computational cells is an unavoidable shortcoming of the VOF method, which can be mitigated utilizing a very refined mesh in the proximity of the interface, together with special numerical treatment of (4) [31]. The comparison of Figures 7 to 8 evidences that the water jets originate from the pressure peak that, in turn, is located at the intersection between the air-water interface and the wedge wall. Therefore, the assumption underlying the ϕ calculation is supported by 2D CFD results. Figure 6(c) shows

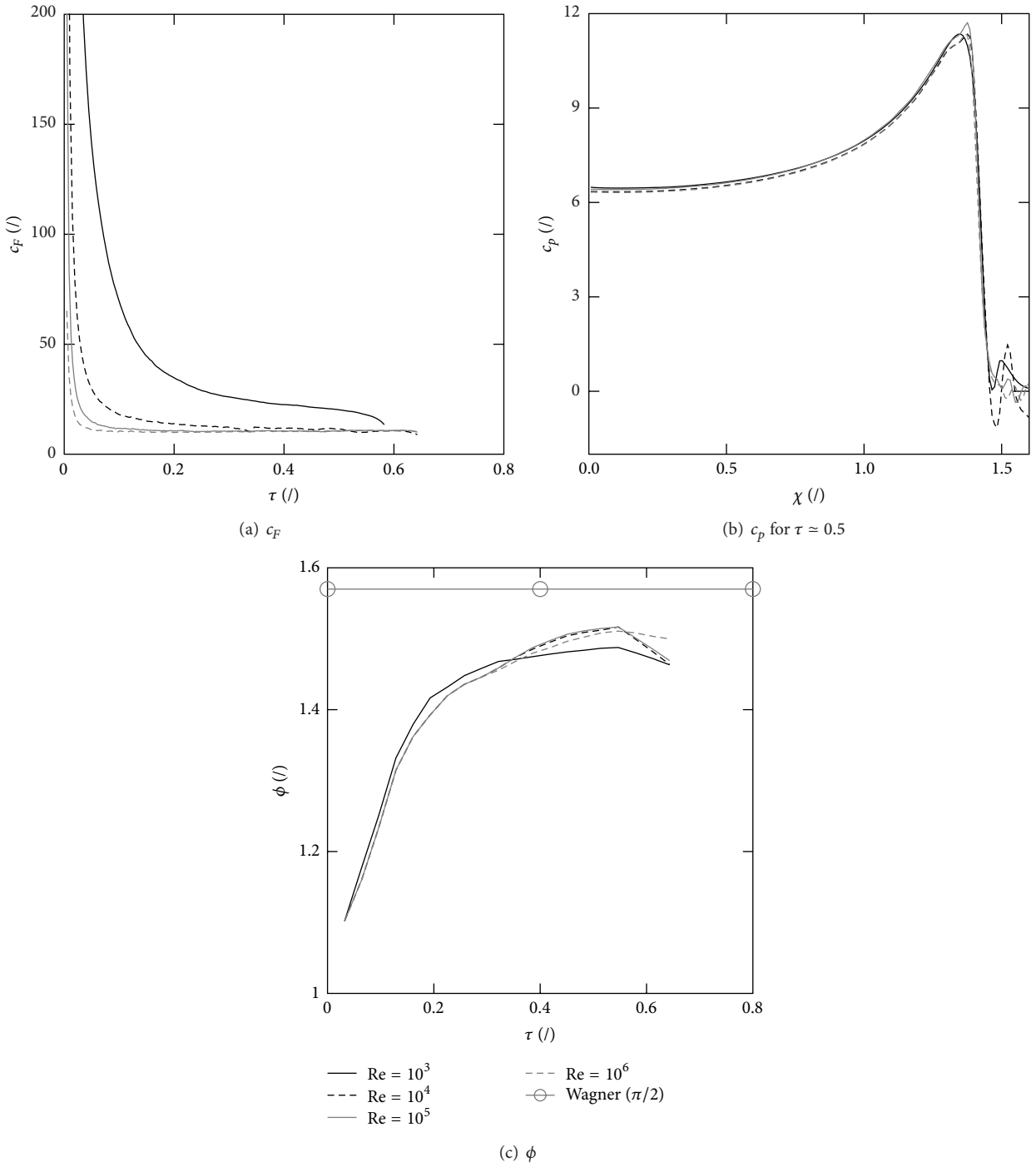

(a) c_F

(b) c_p for $\tau \simeq 0.5$

(c) ϕ

FIGURE 6: Influence of the Reynolds number on the slamming hydrodynamics for Fr = ∞. (a) Force coefficient as a function of the dimensionless time, τ; (b) pressure profile on the wet surface for $\tau = 0.5$ as a function of the dimensionless abscissa, χ; and (c) pile-up coefficient as a function of the dimensionless time, τ.

that ϕ is not influenced by Re, coherently with the analytical results deriving from the potential flow theory [5, 6]. Further evidence of this behavior can be derived from Figure 8 where we observe that the flow pattern remains almost the same in the Reynolds number range 10^3 to 10^6. On the other hand, τ has a decisive effect on the pile-up evolution. Specifically, regardless of the Reynolds number value, ϕ increases with τ with a remarkable rate at the impact onset. The rate of variation of ϕ reduces as τ gets larger, and the pile-up coefficient does not reach the value of $\pi/2$ predicted by Wagner before the wedge is completely submerged. This is confirmed by the experimental observations provided by Panciroli et al. [42]. It is worth noting that analytical and semianalytical approaches, usually assume a constant ϕ [5, 6, 43], while

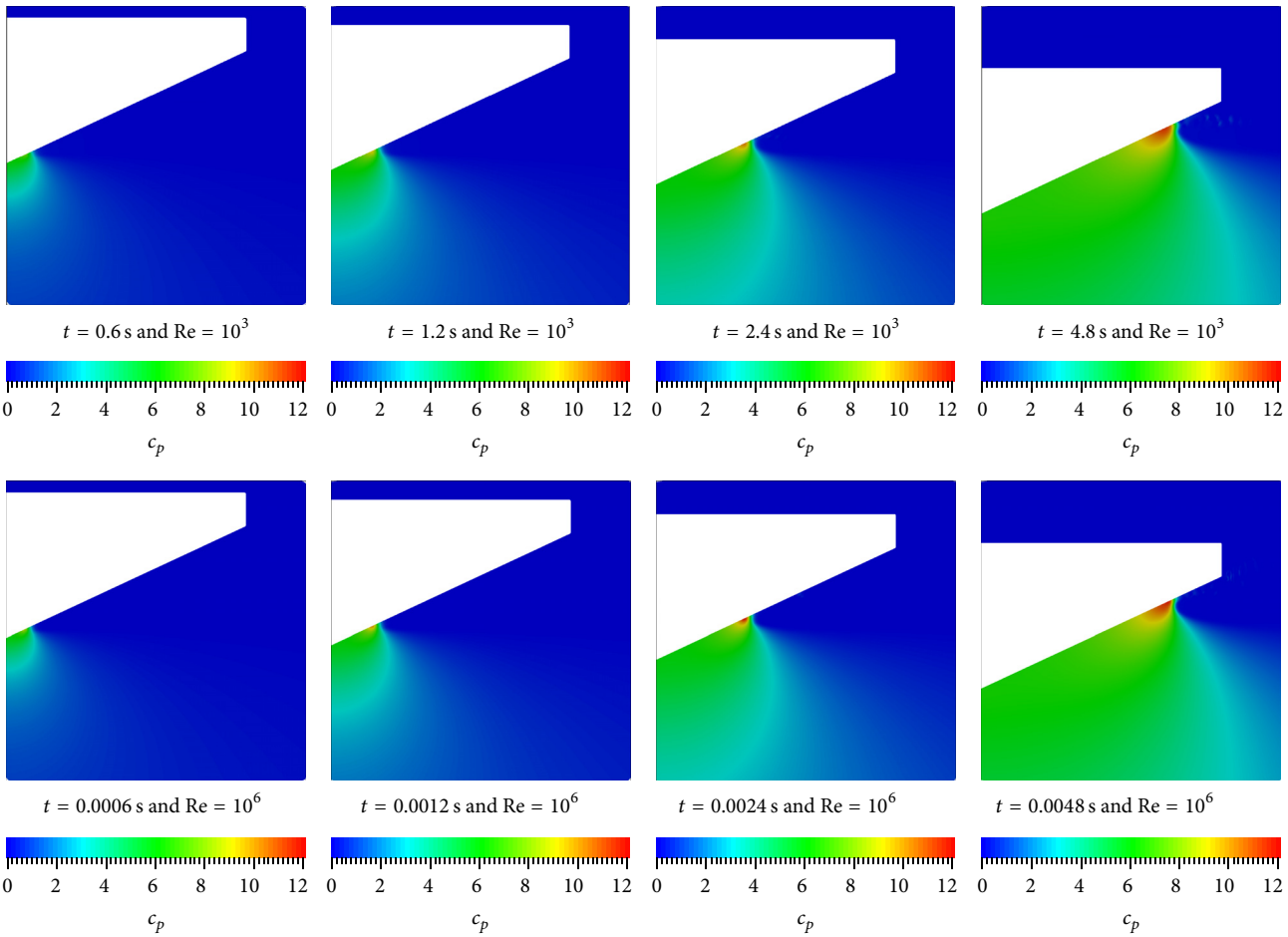

FIGURE 7: Pressure coefficient contour plots for Fr = ∞ as a function of Re and t. Re is increased from bottom to top; t is increased from left to right. Time steps are selected to obtain the same τ values for each Re.

numerical results, supported by the experiments reported in [26, 42], show that ϕ is a function of the wedge penetration.

The interplay between viscous and inertial effects is detectable by investigating the wedge penetration with Fr = 0.5 and varying Re. Results reported in Figure 9 evidence that the same qualitative conclusions derived for Fr = ∞ also apply for Fr < ∞. Specifically, c_p and ϕ are not significantly influenced by the Reynolds number (see Figures 9(b) and 9(c)), which instead affects c_F, in particular at the onset of the water impact (i.e., for small τ). It is worth mentioning that, as a consequence of the wedge acceleration, when Fr < ∞, the c_F curves do not tend to a constant value for large τ. Yet for Re > 10^4, and τ > 0.2, the c_f curves collapse to the same linear function. Moreover, if we compare the results of the sensitivity analysis to Re relative to Fr = ∞ (reported in Figure 6) to the ones relative to Fr = 0.5 (reported in Figure 9) we may substantially exclude mutual influences between Re and Fr.

4.3. Influence of the Generalized Froude Number. In this section we discuss the effects of the generalized Froude number on the hydrodynamics induced by the water entry of the wedge. All the simulations are performed with a constant Re = 10^6 (see Table 2). Thereof, results are not biased by the Re effect, as already discussed in the previous sections. Moreover, being the Reynolds number sufficiently high, the domain of influence of the viscous effects is minimized, as evidenced in Figure 6(a). As in the previous analyses, all the simulations are performed until the wedge is completely submerged, except for the case characterized by a = 100 g, where the motion of the wedge is reversed when the body is not completely submerged, limiting its maximum penetration.

Figure 10 displays the influence of the Froude number on the force coefficient (Figure 10(a)), the pressure profile (Figure 10(b)), and the pile-up coefficient (Figure 10(c)). Results in Figure 10(a) evidence a significant influence of Fr on the pressure coefficient. In particular, excluding the narrow peak close to the slamming onset, c_F exhibits a linear dependence on τ, whose slope increases by raising the deceleration. Moreover, negative c_F values are obtained for a = 100 g in the final part of the numerical experiment, which means that the fluid force is not opposing the wedge penetration. The downward force is the result of the large negative pressure region, clearly visible in Figures 9 and 12.

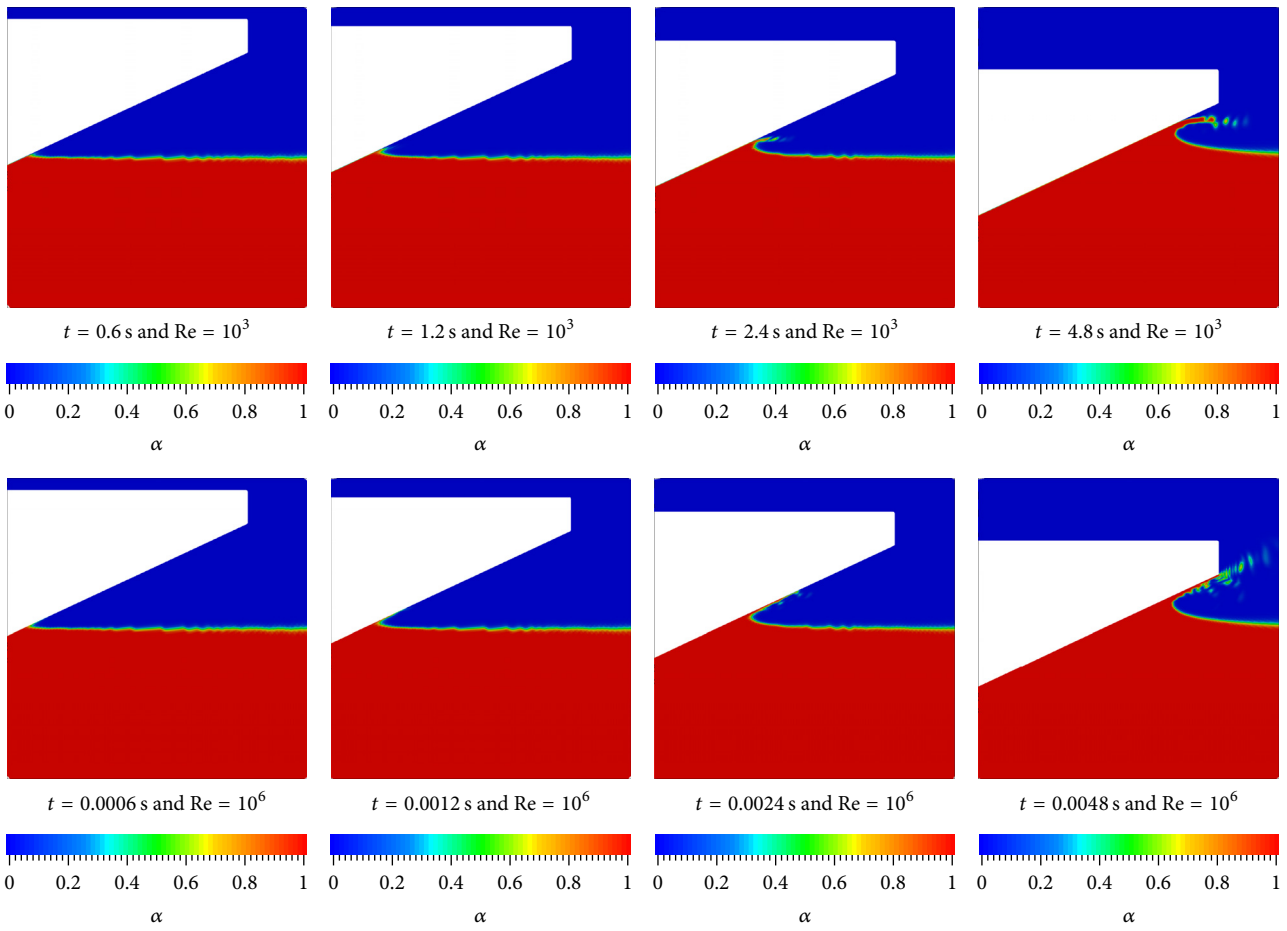

FIGURE 8: Contour plots of the water volume fraction for Fr = ∞ as a function of Re and t. Re is increased from bottom to top; t is increased from left to right. Red color represents water and blue represents air. Time steps are selected to obtain the same τ values for each Re.

Also the pressure profile is influenced by Fr. In particular, as highlighted in Figure 11, by increasing the wedge deceleration, c_p loses the self-similarity in time that characterizes the water entry case with constant downward velocity. Acceleration effects are further clarified in Figure 10(b) that reports c_p for different values of Fr at a constant τ. Specifically, we observe that the pressure peak as well as the keel pressure are reduced by increasing the deceleration. Moreover, the discrepancy between the c_p profiles becomes more evident at larger Froude numbers. On the other hand, the position of the pressure peak is not influenced by Fr. This explains why the pile-up coefficient is not affected by the wedge acceleration, as is clearly detectable from Figure 10(c).

The hydrodynamics related to the wedge impact on the water surface is further explained by the flow fields shown in Figure 12. Therein, the c_p contours for Fr = 7.1 and Fr = 0.5 are reported as a function of τ. In particular the effect of the nondimensional deceleration is clearly evidenced, and the trends of the pressure over the wet surface shown in Figures 10(b) and 11, for the pressure profile on the wet surface of the wedge, are confirmed for the whole c_p field. In fact, the pressure peak is reduced by increasing the deceleration as well as by increasing τ. Moreover, the pressure contour plot for Fr = 0.5 and t = 0.0048 s is of particular interest, as it clearly evidences the presence of a large negative pressure region behind the wedge keel that is also detectable in Figures 10 and 11.

5. Conclusions

In this paper we quantitatively analyze the interplay between inertial, viscous, and pressure effects in water entry problems. In particular, we simulate the impact of a 2D rigid wedge on a quiescent viscous fluid and we assume that the flow is incompressible. The analysis is mainly focused on the effects of nondimensional initial wedge velocity (i.e., Re), acceleration (i.e., Fr), and penetration (i.e., τ). Fr and Re are systematically varied to analyze the interplay between inertial, viscous, and pressure effects on the hull-slamming phenomenon. Such an analysis is performed through the numerical simulation of the water impact of a 2D rigid wedge.

First of all, the numerical model is validated through experimental results available in the literature [4]. The validation process not only confirms the reliability of the numerical procedure, but also evidences that CFD is able to take into consideration several physical aspects that are discarded

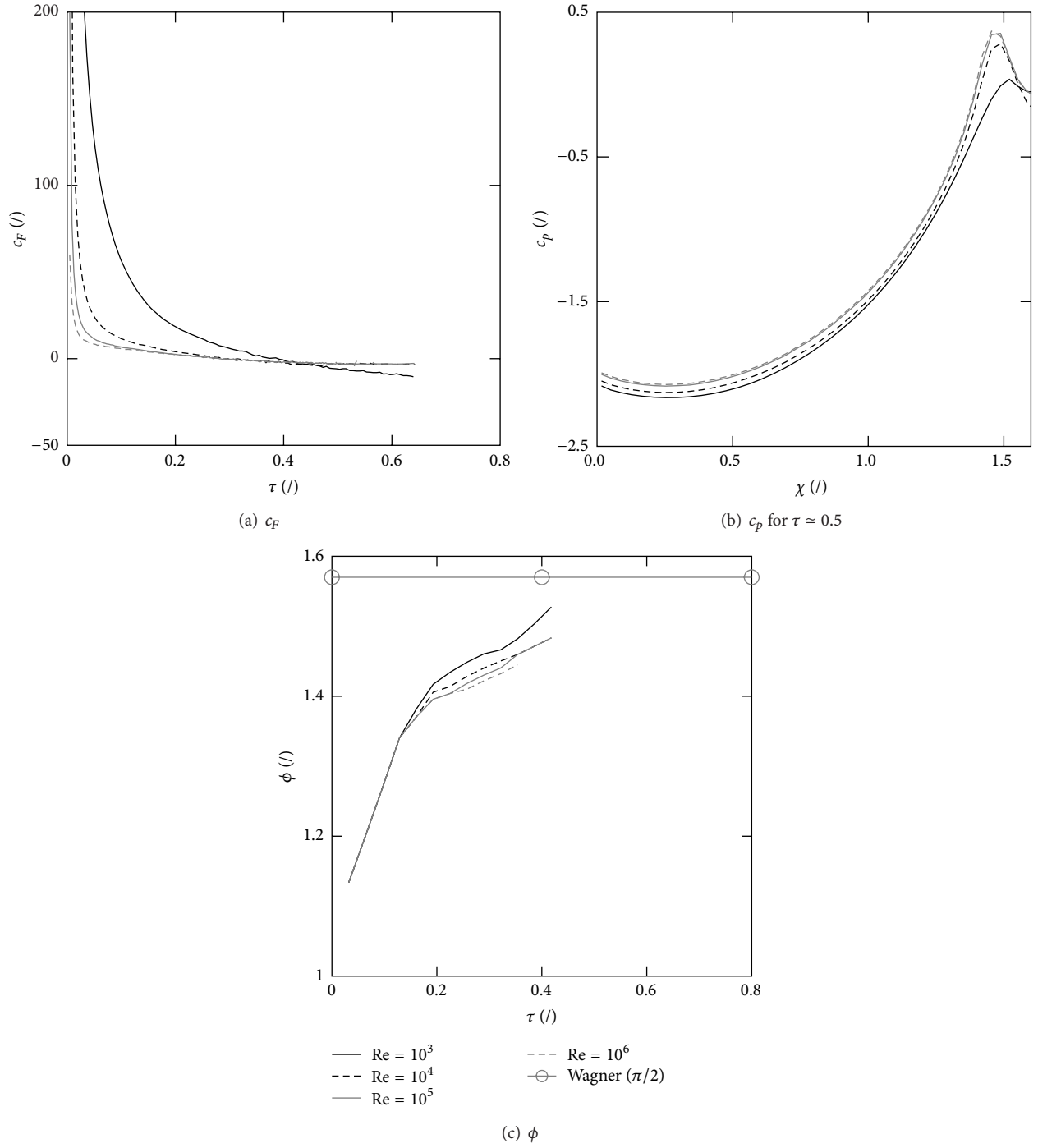

(a) c_F

(b) c_p for $\tau \simeq 0.5$

(c) ϕ

Figure 9: Influence of the Reynolds number on the slamming hydrodynamics for Fr = 0.5. (a) Force coefficient as a function of the dimensionless time, τ; (b) pressure profile on the wet surface for $\tau = 0.5$ as a function of the dimensionless abscissa, χ; and (c) pile-up coefficient as a function of the dimensionless time, τ.

by theoretical approaches. In particular, CFD results are coherent with experimental measurement, in predicting that the minimum value of the pressure is not exactly located on the wedge keel, unlike the analytical models based on the potential flow theory. This discrepancy is particularly evident for the cases characterized by Fr $< \infty$ and is closely related to the hypothesis of small β underlying Wagner's theory. In fact, the small deadrise angle approximation is therein introduced to warrant the usage of a simplified boundary condition for the velocity potential on the wedge surface [1] (i.e., treating the wedge as a flat plate). Removing this simplification allows the pressure minimum to move away from the wedge keel as demonstrated in [8, 9], further confirming the validity of the numerical approach.

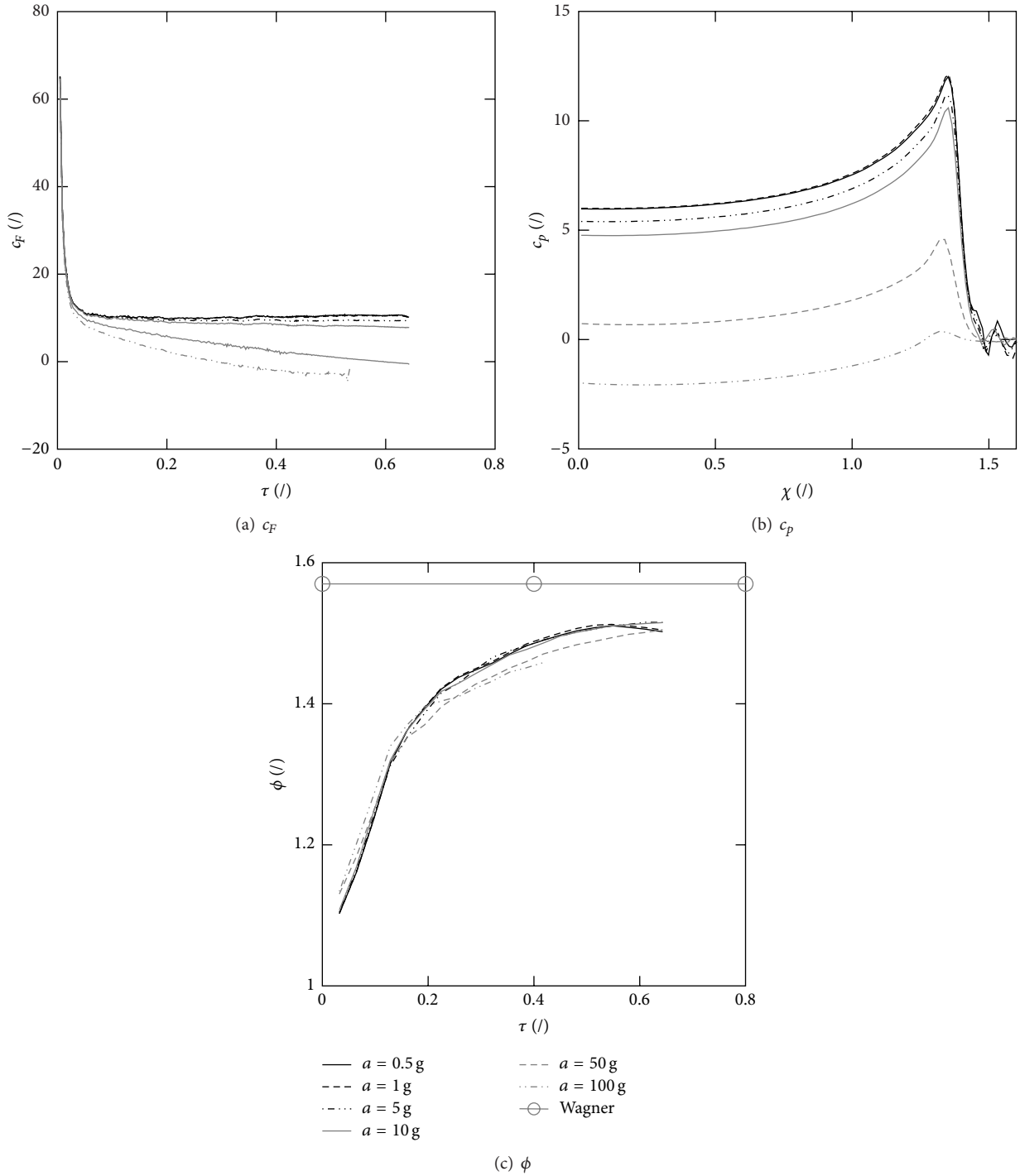

FIGURE 10: Influence of the generalized Froude number on the slamming hydrodynamics for Re = 10^6. (a) Force coefficient as a function of the dimensionless time, τ; (b) pressure profile on the wet surface for $\tau = 0.5$ as a function of the dimensionless abscissa, χ; and (c) pile-up coefficient as a function of the dimensionless time, τ.

Then, a complete set of numerical experiments, reported in Table 2, are performed. Specifically, Re is varied in the range $[10^3, 10^6]$ and Fr in the range $[0.5, \infty)$ to elucidate the influence of each nondimensional parameter in determining the hydrodynamic load generated by the impact. It is evidenced that Fr fundamentally influences both c_F and c_p (see Figure 10). On the other hand Re does not affect c_p (see Figures 6 and 9(b)) and its influence on c_F is limited to a relatively reduced region characterized by $\tau < 1/3$ for Re $> 10^4$. We further comment that, for real world applications, usually, Re is far beyond this threshold limit and that, at the onset of the water slamming, when c_F exhibits a steep

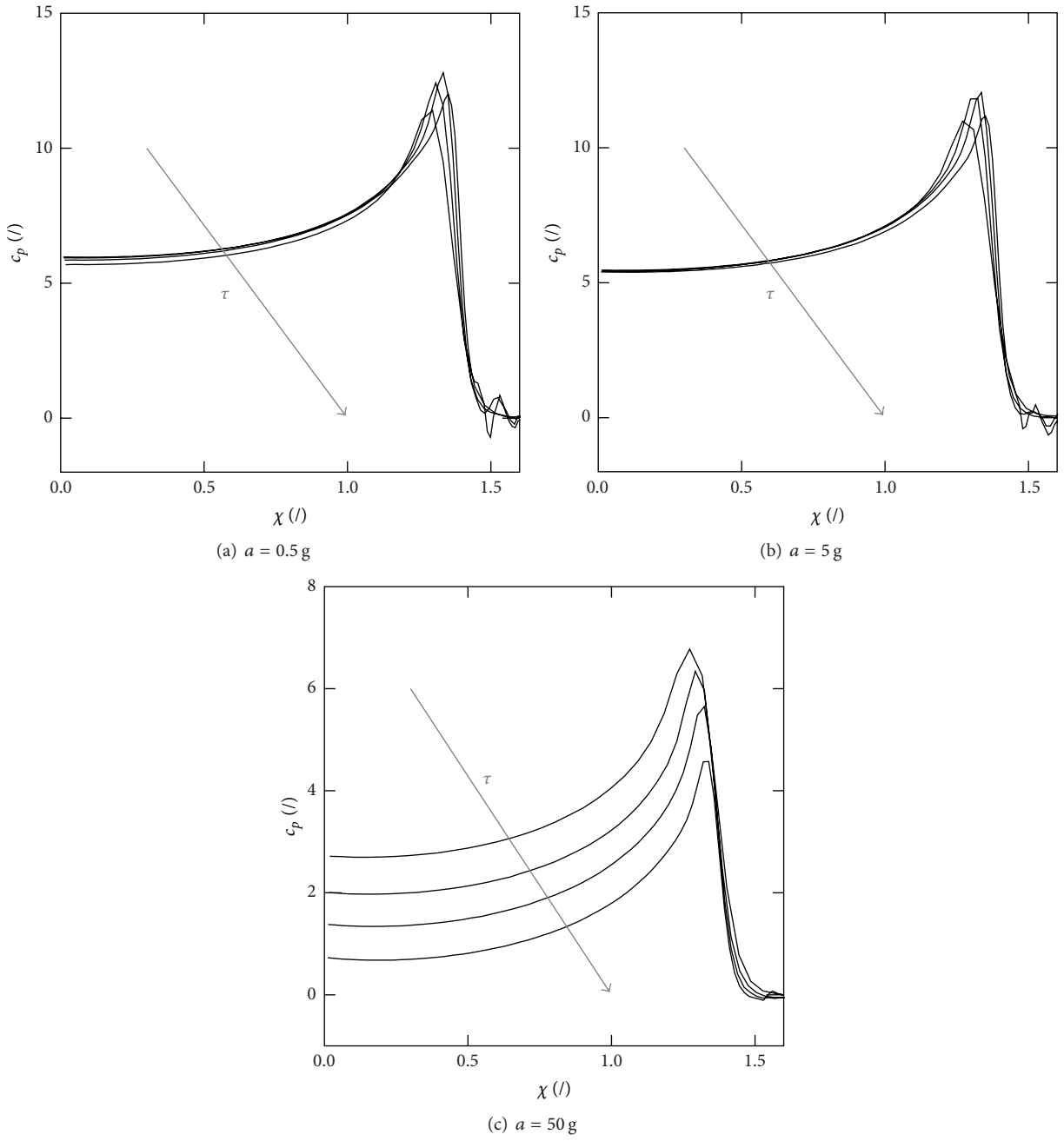

Figure 11: Pressure profile on the wet side of the wedge as a function of χ and τ for Re = 10^6. (a) $a = 0.5$ g; (b) $a = 5$ g; and (c) $a = 50$ g.

dependence on τ and Re, the total slamming force F on the structure is very limited due to the reduced portion of the surface involved. Two sets of numerical experiments on Re effects are performed, (i) Fr = ∞; (ii) Fr = 0.5, and lead to the same considerations, excluding significant mutual influences between these two parameters.

Numerical results also evidenced that the pile-up coefficient is function of the wedge penetration, in contrast with analytical approaches that generally predict a constant value for ϕ. Moreover ϕ is always lower than the value predicted by Wagner, which is $\phi_w = \pi/2$. On the contrary, ϕ is not significantly influenced by Re nor by Fr.

To conclude, this CFD study evidences that, when designing physical as well numerical experiments, under laboratory scale dimensions, or, more generally, utilizing different parameters compared to the real object in study, the experimental parameters must be selected with care. In particular, when the interest lies in structurally relevant hydrodynamic loads: (i) Fr number should be replicated as close as possible in the scaled model, since it plays a fundamental role in the determination of hydrodynamic loads and on the pressure distribution on the solid surface. (ii) Re number similitude is not a stringent constraint, as far as "high Re" is considered. In fact, hydrodynamic loads are

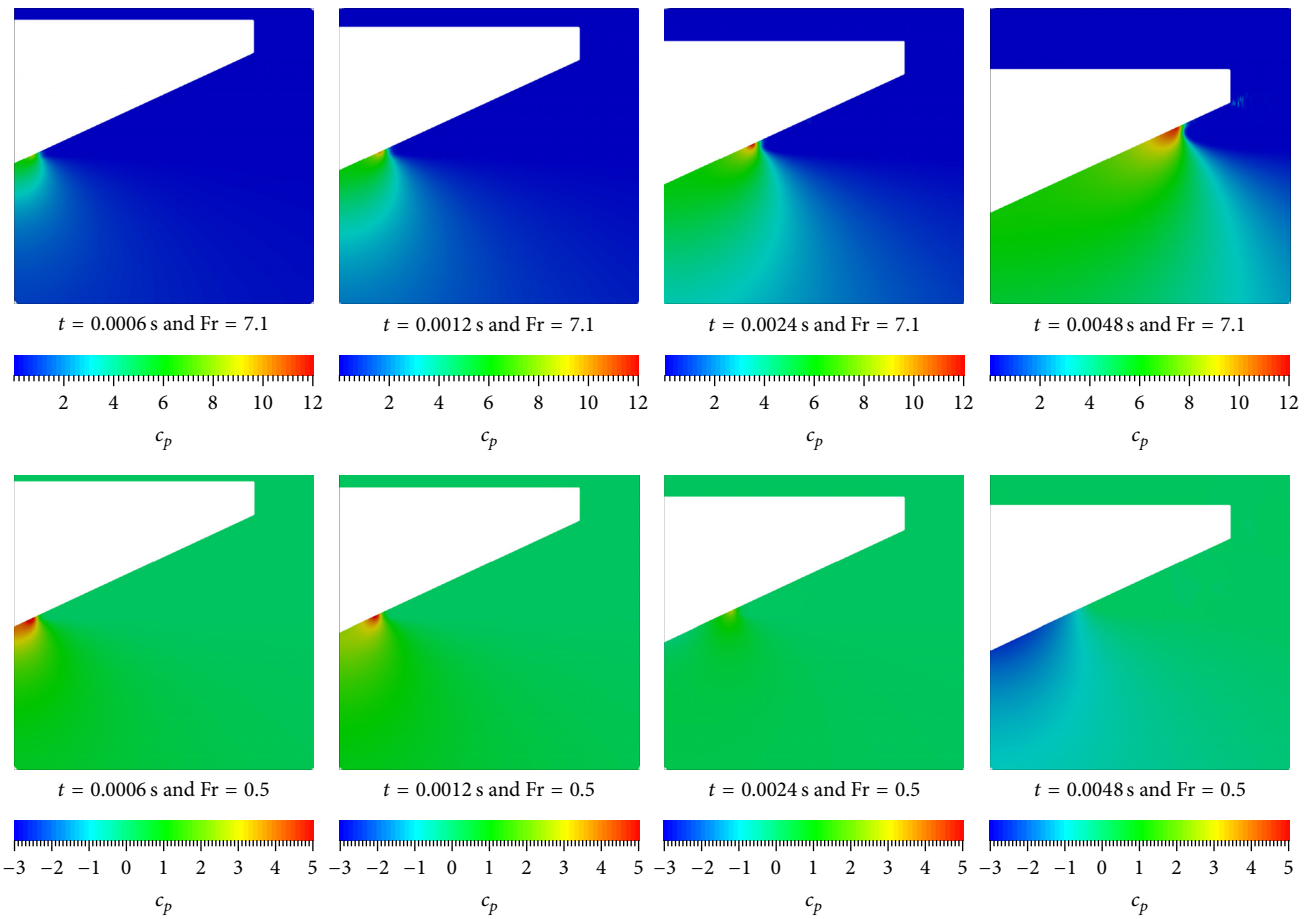

Figure 12: Pressure coefficient contour plots for Re = 10^6 as a function of Fr and t. Fr is increased from bottom to top; t is increased from left to right.

mainly determined by the fluid inertia opposing the wedge motion, and viscosity does not play a determinant role.

Conflict of Interests

The authors declare that there is no conflict of interests regarding the publication of this paper.

References

[1] O. M. Faltinsen, *Hydrodynamics of High-Speed Marine Vehicles*, Cambridge University Press, 2005.

[2] E. Poodts, R. Panciroli, and G. Minak, "Design rules for composite sandwich wakeboards," *Composites Part B: Engineering*, vol. 44, no. 1, pp. 628–638, 2013.

[3] D. van Nuffel, K. S. Vepa, I. de Baere et al., "A comparison between the experimental and theoretical impact pressures acting on a horizontal quasi-rigid cylinder during vertical water entry," *Ocean Engineering*, vol. 77, pp. 42–54, 2014.

[4] R. Panciroli and M. Porfiri, "Evaluation of the pressure field on a rigid body entering a quiescent fluid through particle image velocimetry," *Experiments in Fluids*, vol. 54, no. 12, article 1630, 2013.

[5] T. Von Karman, "The impact on seaplane floats, during landing," Tech. Rep. NACA-TN-321, 1929.

[6] H. Wagner, "Über Stoß- und Gleitvorgänge an der Oberfläche von Flüssigkeiten," *Zeitschrift Für Angewandte Mathematik und Mechanik*, vol. 12, no. 4, pp. 193–215, 1932.

[7] T. Miloh, "On the initial-stage slamming of a rigid sphere in a vertical water entry," *Applied Ocean Research*, vol. 13, no. 1, pp. 43–48, 1991.

[8] R. Zhao and O. Faltinsen, "Water entry of two-dimensional bodies," *Journal of Fluid Mechanics*, vol. 246, pp. 593–612, 1993.

[9] R. Zhao, O. Faltinsen, and J. Aarsnes, "Water entry of arbitrary twodimensional sections with and without flow separation," in *Proceedings of the 21st Symposium on Naval Hydrodynamics*, pp. 408–423, Trondheim, Norway, June 1996.

[10] E.-M. Yettou, A. Desrochers, and Y. Champoux, "A new analytical model for pressure estimation of symmetrical water impact of a rigid wedge at variable velocities," *Journal of Fluids and Structures*, vol. 23, no. 3, pp. 501–522, 2007.

[11] A. Iafrati and A. A. Korobkin, "Hydrodynamic loads during early stage of flat plate impact onto water surface," *Physics of Fluids*, vol. 20, no. 8, Article ID 082104, 2008.

[12] Y. A. Semenov and B.-S. Yoon, "Onset of flow separation for the oblique water impact of a wedge," *Physics of Fluids*, vol. 21, no. 11, Article ID 014911PHF, pp. 1–11, 2009.

[13] A. Tassin, A. Korobkin, and M. Cooker, "On analytical models of vertical water entry of a symmetric body with separation and cavity initiation," *Applied Ocean Research*, vol. 48, pp. 33–41, 2014.

[14] R. Panahi, E. Jahanbakhsh, and M. S. Seif, "Development of a VoF-fractional step solver for floating body motion simulation," *Applied Ocean Research*, vol. 28, no. 3, pp. 171–181, 2006.

[15] R. Panciroli, S. Abrate, G. Minak, and A. Zucchelli, "Hydroelasticity in water-entry problems: comparison between experimental and SPH results," *Composite Structures*, vol. 94, no. 2, pp. 532–539, 2012.

[16] S. Seng, J. J. Jensen, and P. T. Pedersen, "Numerical prediction of slamming loads," *Proceedings of the Institution of Mechanical Engineers, Part M: Journal of Engineering for the Maritime Environment*, vol. 226, no. 2, pp. 120–134, 2012.

[17] A. D. Rosis, G. Falcucci, M. Porfiri, F. Ubertini, and S. Ubertini, "Hydroelastic analysis of hull slamming coupling lattice Boltzmann and finite element methods," *Computers & Structures*, vol. 138, pp. 24–35, 2014.

[18] R. Marcer, C. Berhault, C. de Jouëtte, N. Moirod, and L. Shen, "Validation of CFD codes for slamming," in *Proceedings of the European Conference on Computational Fluid Dynamics (ECCOMAS CFD '10)*, pp. 14–17, 2010.

[19] M. Rahaman, K. Zheng, and H. Akimoto, "Numerical investigation of bow slamming on ships with large flare," in *Proceedings of the MARTEC*, 2010.

[20] R. Panciroli, "Water entry of flexible wedges: some issues on the FSI phenomena," *Applied Ocean Research*, vol. 39, pp. 72–74, 2013.

[21] R. Panciroli, S. Abrate, and G. Minak, "Dynamic response of flexible wedges entering the water," *Composite Structures*, vol. 99, pp. 163–171, 2013.

[22] R. Panciroli and M. Porfiri, "Hydroelastic impact of piezoelectric structures," *International Journal of Impact Engineering*, vol. 66, pp. 18–27, 2014.

[23] A. El Malki Alaoui, A. Nême, A. Tassin, and N. Jacques, "Experimental study of coefficients during vertical water entry of axisymmetric rigid shapes at constant speeds," *Applied Ocean Research*, vol. 37, pp. 183–197, 2012.

[24] D. van Nuffel, K. S. Vepa, I. de Baere, J. Degrieck, J. de Rouck, and W. van Paepegem, "Study on the parameters influencing the accuracy and reproducibility of dynamic pressure measurements at the surface of a rigid body during water impact," *Experimental Mechanics*, vol. 53, no. 2, pp. 131–144, 2013.

[25] J. Shahraki, I. Penesis, G. Thomas, M. Davis, and J. Whelan, "Prediction of slamming behaviour of monohull and multihull forms using smoothed particle hydrodymamics," in *Proceedings of the 9th Symposium on High Speed Marine Vehicles (HSMV '11)*, vol. 400, pp. 1–10, Naples, Italy, May 2011.

[26] A. L. Facci, R. Panciroli, S. Ubertini, and M. Porfiri, "Assessment of PIV-based analysis of water entry problems through synthetic numerical datasets," *Journal of Fluids and Structures*, vol. 55, pp. 484–500, 2015.

[27] E. Buckingham, "On physically similar systems; Illustrations of the use of dimensional equations," *Physical Review*, vol. 4, no. 4, pp. 345–376, 1914.

[28] ESI, 2014, http://www.openfoam.com/.

[29] W. J. Rider and D. B. Kothe, "Reconstructing volume tracking," *Journal of Computational Physics*, vol. 141, no. 2, pp. 112–152, 1998.

[30] R. Scardovelli and S. Zaleski, "Direct numerical simulation of freesurface and interfacial flow," *Annual Review of Fluid Mechanics*, vol. 31, no. 1, pp. 567–603, 1999.

[31] H. Rusche, *Computational fluid dynamiccs of dospersed twophase flows at high phase fractions [Ph.D. thesis]*, 2002.

[32] C. Biscarini, S. Di Francesco, and P. Manciola, "CFD modelling approach for dam break flow studies," *Hydrology and Earth System Sciences*, vol. 14, no. 4, pp. 705–718, 2010.

[33] C. Biscarini, S. Di Francesco, F. Nardi, and P. Manciola, "Detailed simulation of complex hydraulic problems with macroscopic and mesoscopic mathematical methods," *Mathematical Problems in Engineering*, vol. 2013, Article ID 928309, 14 pages, 2013.

[34] S. Patankar, *Numerical Heat Transfer and Fluid Flow*, Series on Computational Methods in Mechanics and Thermal Sciences, Taylor & Francis, 1980.

[35] R. I. Issa, "Solution of the implicitly discretised fluid flow equations by operator-splitting," *Journal of Computational Physics*, vol. 62, no. 1, pp. 40–65, 1986.

[36] OpenFOAM Foundation, *OpenFOAM User's Guide*, OpenFOAM Foundation, Boston, Mass, USA, 2013.

[37] H. Jasak, H. G. Weller, and A. D. Gosman, "High resolution NVD differencing scheme for arbitrarily unstructured meshes," *International Journal for Numerical Methods in Fluids*, vol. 31, no. 2, pp. 431–449, 1999.

[38] OpenFOAM Foundation, *OpenFOAM Programmer's Guide*, OpenFOAM Foundation, Boston, Mass, USA, 2013.

[39] H. Jasak and Ž. Tuković, "Automatic mesh motion for the unstructured finite volume method," *Transactions of FAMENA*, vol. 30, no. 2, pp. 1–20, 2006.

[40] H. Jasak, "Dynamic mesh handling in OpenFOAM," in *Proceedings of the 47th AIAA Aerospace Sciences Meeting Including the New Horizons Forum and Aerospace Exposition*, Orlando, Fla, USA, January 2008.

[41] C. Kassiotis, "Which strategy to move the mesh in the computational fluid dynamic code OpenFOAM?" Tech. Rep., WiRe, Düsseldorf, Germany; LMT Cachan, Cachan, France, 2008, http://perso.crans.org/kassiotis/openfoam/movingmesh.pdf.

[42] R. Panciroli, A. Shams, and M. Porfiri, "Experiments on the water entry of curved wedges: high speed imaging and particle image velocimetry," *Ocean Engineering*, vol. 94, pp. 213–222, 2015.

[43] A. Korobkin, "Analytical models of water impact," *European Journal of Applied Mathematics*, vol. 15, no. 6, pp. 821–838, 2004.